Solar Energy 304 (2026) 114194

Contents lists available at ScienceDirect

Solar Energy

journal homepage: www.elsevier.com/locate/solener

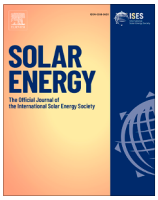

Volumetric flow determination in parabolic trough plants using the time offset of temperature gradients

Alex Brenner[a,b,*], Tobias Hirsch[a], Marc Röger[c], Jana Stengler[a], Robert Pitz-Paal[b,d]

[a] German Aerospace Center (DLR), Institute of Solar Research, Pfaffenwaldring 38-40, Stuttgart, 70569, Germany
[b] RWTH Aachen University, Chair of Solar Technology, Linder Höhe, Cologne, 51147, Germany
[c] German Aerospace Center (DLR), Institute of Solar Research, Calle Doctor Carracido 44-1, Almería, E-04005, Spain
[d] German Aerospace Center (DLR), Institute of Solar Research, Linder Höhe, Cologne, 51147, Germany

HIGHLIGHTS

- Time delay of temperature signals indicates current flow in parabolic trough plants.
- Allows determination of absolute value of volume flow without additional hardware.
- Low-cost alternative to classical flow measurement instruments.
- Validated using data from a commercial thermal oil CSP plant during operation.
- Mean deviation from measured subfield flow in Andasol-3 plant is 6.15 %.

ARTICLE INFO

Keywords:
Fluid flow
Parabolic trough
Virtual sensor
Time-of-flight method

ABSTRACT

The absence of flow measurements in the loop of a parabolic trough solar field makes it impossible to easily determine flow for the purpose of calculating the performance of a loop. This proof-of-concept study uses the temperature signals of the heat transfer fluid, measured at the parabolic trough collectors to determine the runtime of a temperature signal and thus, to infer the runtime of the fluid. It is not dependent on additional measurement instrumentation and only requires data analysis using the available measurement equipment. The approach can be applied to existing parabolic trough loops at nearly no additional cost and could also be used in other pipe flows in process engineering applications. The method is validated in a realistic application scenario with data from the parabolic trough power plant Andasol-3 and shows a mean absolute percentage error of 6.15 % compared to the measured subfield mass flow.

1. Introduction

The steady-state useful power in a parabolic trough collector is measured in practice by determining the inlet and outlet temperature and the mass flow rate of the heat transfer fluid (HTF). The former can be approximated with the built-in temperature sensors at the collectors, but the latter is usually not available in a regular parabolic trough loop. This absence of a mass flow meter has made power estimations without additional measurement instrumentation impossible until now.

The paper describes an approach for determining the volumetric flow rate based on the runtime of a temperature signal carried by the HTF in a parabolic trough loop. The runtime of the fluid is calculated using time differences of temperature signals together with a correction function to account for heat transfer and thermal inertia of the pipe and fluid. The challenge in using this approach is that the time difference observed between two temperature measurement locations cannot simply be assigned to a fluid velocity. The reason for this is that heat transfer and thermal inertia of the pipe and fluid shift and dampen the original temperature signal.

Line-focusing solar thermal power plants usually consist of four to six collectors connected in series to form so-called loops. In commercial parabolic trough plants for electricity generation a large number of approximately 40 loops are connected in parallel and form a subfield. Due to the high number of parallel loops, there is usually only one volumetric flow measurement for each subfield, but not for each parallel loop. However, for various applications it is advantageous to know the flow

* Corresponding author at: German Aerospace Center (DLR), Institute of Solar Research, Pfaffenwaldring 38-40, Stuttgart, 70569, Germany.
Email address: alex.brenner@dlr.de (A. Brenner).

https://doi.org/10.1016/j.solener.2025.114194
Received 25 April 2025; Received in revised form 31 October 2025; Accepted 25 November 2025
Available online 3 December 2025

of the HTF in each loop. Examples include the hydraulic balancing of the loop inlet valves during commissioning, the continuous monitoring of the collector performance, or collector-specific control tasks, which require knowledge about the flow in each individual loop. To determine the volumetric flow in parallel pipes, such as those in parabolic trough power plants, a separate volumetric flow meter would be required for each individual pipe. These measuring devices are either installed as a stationary device in the fluid flow, or can be attached to the outer wall of the pipe as a flexible device. The usual operating principles of these meters are based on:

- Transit time measurements of acoustic signals
- Measurement of a pressure difference before and after an orifice plate
- Measurement of the vortex frequency after an interference body
- Magnetic-inductive measurement in an electrically conducting medium

These devices are very costly in the range of 5000 €per unit. For a parabolic trough field with a power of 50 MW and about 150 parallel loops, this sums up to $150 \times 5000\,€ = 750{,}000\,€$. Because of the high cost of using measuring devices in each loop, the installation has generally been omitted up to now since main collector control tasks can be realized based on temperature signals alone. Moreover, each device inserted into the fluid flow disturbs it, adds pressure loss and increases the probability that one of these devices will fail. The use of an approach for volume flow determination that utilizes existing measurement instrumentation and solar collectors can therefore be advantageous.

For the control and monitoring of the collectors, temperature sensors are usually installed on each collector, see [1]. The collectors are able to adjust the heat input, by rotating the collector axis. This is part of the control system in order to react to changes in fluid flows in the receiver and local irradiation fluctuations. The change in heat input is described by the focus factor, which can have values from 0 representing no heat input to 1 representing the maximum possible heat input. By changing the focusing and therefore the heat input, the temperature of the fluid can also be actively controlled. Fig. 1 shows that a small rotation $\Delta\varrho$ of the collector tracking axis leads to a focus factor reduction resulting in a temperature drop, which is measurable at all temperature sensors in the loop with a time delay. The curves in the right panel of Fig. 1 show the temperature values in the collector middle and are the results of a simulation with constant DNI of 800 W m^{-2}, a time step of 0.1 s, and complete defocusing of collector 1 for 200 s.

The general idea of the method in this work is to observe temperature signals measured at two positions along the collector loop and to determine the time shift between the signals. The requirement is that both locations observe the same ramp in the temperature signal. Such a signal can either be caused by changes in solar irradiance or artificially imposed by a change in collector tracking. The latter approach results in undisturbed signals that can be clearly detected as a temperature disturbance. A fluid element flowing through the loop also carries the temperature information. This makes it possible to measure the time delay of temperature signals at two or more temperature sensors in a loop. The volume flow rate can be inferred from this time delay, taking into account inertia effects in the pipe section between the two measuring points. The influence of the thermal inertia on the temperature signals is calculated in this work using a deterministic transient model for parabolic trough fields. This model is employed to simulate the behavior of a real parabolic trough field and thus to easily transfer the approach presented here to a real plant. The implementation of this procedure is very cost-effective, as only software is required. Furthermore, there is no need to modify the piping, and the operation of the plant is not disturbed. It is therefore assumed that the procedure has a low threshold for implementation by the power plant operators and can thus be used in a variety of ways.

1.1. State of the art

Using the runtime of a temperature signal in order to infer the flow has already been investigated in multiple studies in other technical setups. Bauer [2] uses a heating and a sensing wire in a gas stream together with a pulsed heating current to measure the velocity of the fluid flow. A similar approach is described by [3,4]. All these approaches are investigated in gas streams with comparatively small heat capacities and the influence of a surrounding pipe is neglected due to the chosen experimental setups. Another application of the temperature runtime method is heat pulse flow meters, as described by [5]. These devices are used to measure the velocity of ground water in a bore hole. Although this approach is made for liquid fluids the typical velocities are in the range of 5 mm s^{-1} to 30 mm s^{-1} and therefore orders of magnitude smaller than in a parabolic trough loop. Research activities for special applications in nuclear power plants investigated a similar procedure, using the temperature signals in fluids, as described in [6,7]. In these setups, the distances between the temperature sensors are 2 mm up to 2.05 m and therefore much smaller than the 150 m that is common in thermal oil parabolic trough loops. The influence of the pipe wall is therefore neglected in these publications. Nedumparambil et al. [8] show an application of the temperature runtime method in low-temperature solar thermal applications. The distance between the temperature sensors here is 0.48 m. Due to the small measurement distance, the influence of the heat capacity of the pipe material on the temperature signal is neglected in this publication. Mehos et al. [9] mention a procedure used in a parabolic trough power plants where the temperature sensors are used to measure

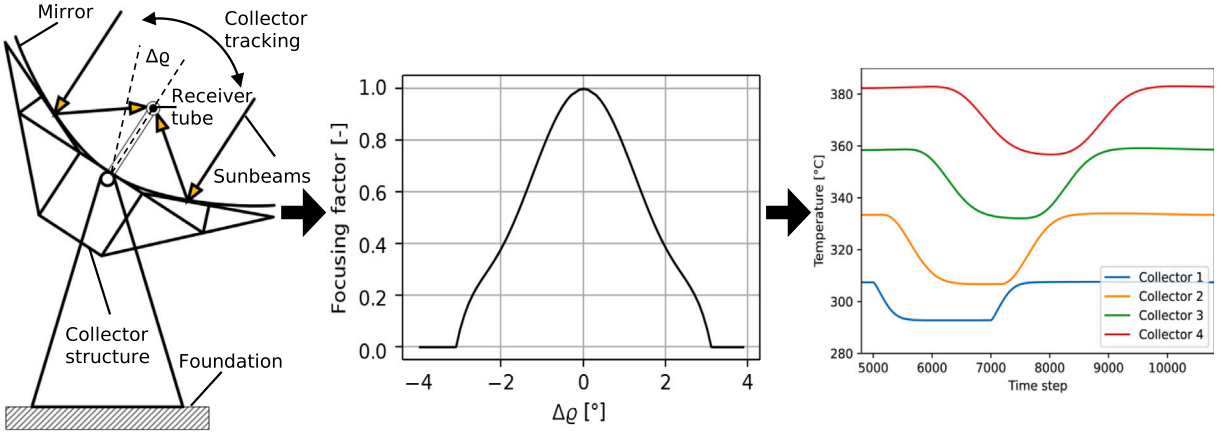

Fig. 1. Illustration of collector defocusing procedure. Left: Schematic side view of parabolic trough collector. Middle: Dependency of the focus factor from tracking angle deviations. Right: Temperature drop can be measured at all collectors in the loop with a time delay.

the flow in each loop. However, there is no additional information, nor any publication about this procedure available. In the context of concentrating solar power plants, the recently published papers by [10,11] describe a time-of-flight method using a temperature signal. Kraft et al. [10] use a temperature signal, which is caused by warm fluid entering the solar loops from the header pipe during the start-up phase in the morning to demonstrate the approach. They also mention an artificially forced temperature change caused by briefly defocusing individual collectors during operation. In Kraft et al. [11] the method is applied to a temperature signal created by temporarily focusing or defocusing a collector in a test facility. The procedure makes it possible to determine a linear relationship between the temperature signal time-of-flight and the mass flow. To determine the absolute fluid flow for a single loop or a single collector, an additional flow meter is required, at least temporarily for individual calibration purposes. The study also addresses thermal inertia effects, e.g., caused by the pipe wall. Our work builds on this study and expands upon it.

The literature review shows that there are currently still some gaps that prevent the implementation of the method in real parabolic trough power plants. The approaches mentioned above have either not been developed for a liquid medium with comparatively high heat capacity, do not take into account the influence of the pipe wall in contact with the medium, are not described in the literature available to the authors, or are not capable of calculating the absolute value of fluid flow. Therefore, in the following an approach is presented, which allows to be used at the conditions occurring in parabolic trough loops and is able to determine absolute values of fluid flow for each loop individually.

1.2. Structure of the paper

Section 2.1 discusses the influencing effects on the time offset of the temperature signals, followed by an explanation of the practical application of the method in Section 2.2. In Section 2.3 the used approach for determining the time offset of two temperature signals is presented. This provides the basis for determining a time offset from the pure temperature measurements. Subsequently in Section 2.4, the software used for the transient simulations of the solar field is presented. In the results Section 3.2 a correction function based on multiple transient simulations is fitted to determine the runtime of the fluid from the temperature signal. Practitioner plots in Section 3.3 make the procedure easily adaptable for field measurements in the parabolic trough plant. The performance of the method is investigated in both steady-state and transient situations using measured, spatially resolved irradiance data, see Section 3.4. Finally, the method is validated in a realistic application scenario in the Andasol-3 power plant Section 3.5 and the effects of the method on plant operation are the subject of Section 3.6.

2. Methods

In the following, the influencing effects on the time offset of the temperature signals and the practical application of the method are explained. Two important methods that form the basis for the procedure presented in this paper are explained below. On the one hand, the exact determination of the time offset of the HTF temperature signals at the collectors. On the other hand, the transient simulations, which are used to solve the inverse problem of determining the fluid transit time from the temperature transit time.

2.1. Theoretical considerations on the impact of thermal inertia

The underlying principle discussed in this paper is based on the hypothesis that it is possible to determine the time interval between two temperature signals and use it to infer the fluid transit time t_{Fluid}. With known spatial distance between the temperature sensors $l_{1,2}$ and known pipe cross-section A_{pipe} the volumetric flow rate $\dot{V}$ can be calculated as

$$\dot{V} = \frac{V}{t_{\text{Fluid}}} = \frac{A_{\text{pipe}} \cdot l_{1,2}}{t_{\text{Fluid}}} = \frac{\pi/4 \cdot d_{\text{i}}^2 \cdot l_{1,2}}{t_{\text{Fluid}}}. \tag{1}$$

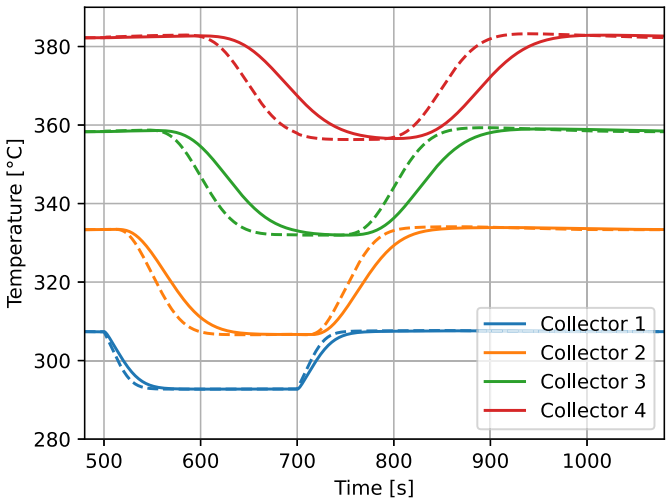

Fig. 2. Illustration of the backwards shift of the temperature signals due to the thermal inertia of the pipe material. Solid lines represent a regular steel pipe with a volumetric heat capacity of 4017 kJ m^{-1} K^{-3}, dashed lines represent an artificial material with a volumetric heat capacity of 192 kJ m^{-1} K^{-3}.

With known fluid density ρ_{Fluid} the mass flow $\dot{m}$ can be calculated from the volumetric flow $\dot{V}$ according to

$$\dot{m} = \dot{V} \cdot \rho_{\text{Fluid}}. \tag{2}$$

A correction function is needed because the thermal inertia of the pipe is high enough to influence the fluid temperature. An approximation of the influence of the thermal inertia of the pipe wall material on the fluid temperature is calculated via a ratio of heat capacities

$$\frac{C_{\text{Pipe}}}{C_{\text{Fluid}}} = \frac{\rho_{\text{Pipe}} \cdot c_{\text{p, Pipe}} \cdot V_{\text{Pipe}}}{\rho_{\text{Fluid}} \cdot c_{\text{p, Fluid}} \cdot V_{\text{Fluid}}} = \frac{\rho_{\text{Pipe}} \cdot c_{\text{p, Pipe}} \cdot \left(d_{\text{o}}^2 - d_{\text{i}}^2\right)}{\rho_{\text{Fluid}} \cdot c_{\text{p, Fluid}} \cdot d_{\text{i}}^2} = 0.269 \tag{3}$$

of an oil trough setup. The densities of pipe material and fluid in this example are $\rho_{\text{Pipe}} = 7792$ kg m^{-3} and $\rho_{\text{Fluid}} = 759.7$ kg m^{-3}, $c_{\text{p, Pipe}} = 516$ J kg^{-1} K^{-1} and $c_{\text{p, Fluid}} = 2454.7$ J kg^{-1} K^{-1} are specific heat capacities of pipe and fluid, and $d_{\text{o}} = 0.07$ m and $d_{\text{i}} = 0.066$ m are outer and inner pipe diameters. The calculation assumes X6CrNiTi18-10 steel as pipe material and Therminol VP-1 at 350 °C as fluid. For the exemplary design point, the heat capacity of the pipe wall is approximately 27 % of the fluid heat capacity and, assuming a reasonably high heat transfer, an influence on the fluid temperature from the pipe and vice versa is obvious.

Fig. 2 shows the calculated effect of thermal inertia on the time offset of the temperature signals from the HTF determined at the collectors. The solid lines represent calculations with regular steel absorber tubes, while the dashed curves show a generic material that has only about 5 % of the volumetric heat capacity of steel. Due to the higher heat capacity of the pipe material the temperature signal is shifted backwards. The temperature curves shown here are calculated using the same model as described in Section 2.4.

2.2. Practical application of the approach

To make the practical application of the approach clear, the individual steps of the process are explained below.

2.2.1. Step 0: transient simulations

Before the actual measurement of the fluid temperatures, a large number of transient simulations are carried out, which represent the expected thermal and flow conditions in the system. The results of these simulations are then used to create a correction function that captures

the relationship between the measured transit time of the temperature signal and the true fluid transit time. If the conditions in the system remain constant, these simulations only need to be carried out once in advance.

2.2.2. Step 1: Runtime of the temperature signal

The temperature gradients in the fluid are measured and the transit time of the signal between two sensors is determined. The temperature gradient can be generated passively by incoming cold fluid or actively by defocusing the collector.

2.2.3. Step 2: Application of the correction function

To determine the fluid transit time, the correction function can now be applied using the transit time of the temperature signal and the available system parameters. Diagrams are created for typical system configurations of parabolic trough power plants with thermal oil. This makes it easy to read out the fluid transit time from the transit time of the temperature signal.

2.3. Gradient detection for time offset calculation of temperature signals

One of the basic conditions for the application of the method described in this paper is the reliable determination of the time offset between the temperature signals at two successive collectors. This work uses the maximum gradients of two temperature signals generated by defocusing the collector and determines the time delay between these two signals. Fig. 3 illustrates the temperature signals with the linearized gradients and the calculation of the time difference t_{Temp}. For this method, the first step is to determine the position of the maximum gradient, i.e., the steepest part of the descending temperature slope. The temperature signal is linearized at this point and the intersection with the maximum, undisturbed temperature T_{norm} just before defocusing is located. The time difference between these two intersection points is taken as the time difference of the two signals. The linearized maximum gradient method (LMG) assumes that the two compared signals are stationary, i.e., the temperature curves have a constant time offset over the signal duration. Due to the determination of the intersection point, the calculated time shift is not constrained to the temporal resolution of the input signals and can be calculated as a fraction of a time step.

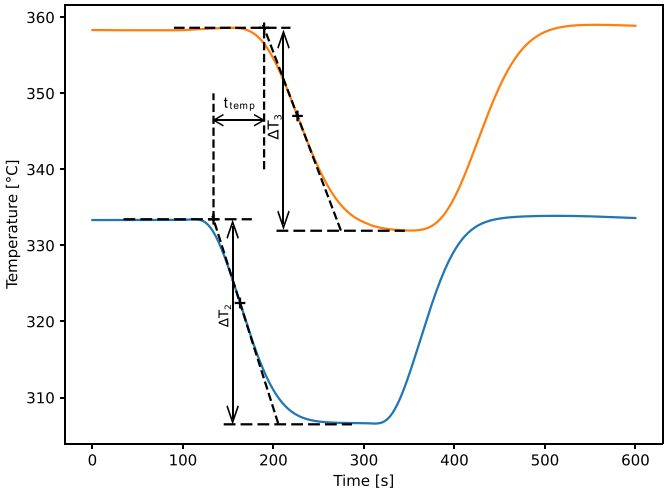

Fig. 3. Linearized maximum temperature gradients method illustrated with a smooth signal of the second (blue) and third collector (orange). The time difference of the temperature signals t_{Temp} is determined by the intersections between undisturbed temperatures before the step and linearized maximum gradients of the temperature steps ΔT_2 and ΔT_3. (For interpretation of the references to colour in this figure legend, the reader is referred to the web version of this article.)

A preliminary study has shown that other methods, such as cross-correlation and dynamic time warping, are also suitable, see [12]. However, these are not used in this work because they are more complicated than the gradient detection method, which, for smooth signals, provides results comparable to those of the more complicated methods.

2.4. Transient simulations

A forward problem modeled with transient simulations calculates the system behavior based on known inputs. In contrast, the inverse problem seeks to infer unknown parameters or inputs from observed data, which makes it more complex because it infers from effects back to causes. The forward problem involves calculating the runtime of the temperature signal for a wide range of variations that represent typical plant conditions using transient simulations. A data-based inverse model is used to determine fluid runtime from observed temperature data and plant parameters, solving the inverse problem.

There are basically two options for determining the fluid runtime using the temperature runtime method: With the help of experiments at a real plant or with transient simulations. The former has the advantage of being close to the operating conditions in a real plant. The major drawbacks are: First of all this procedure requires accurate measurement devices, e.g., accurate flow measurements for comparison, and second, it is not flexible since the components in the test facility cannot be changed easily. The results would thus only be usable for a specific plant configuration. Conducting experiments with changing material properties would be very costly, or even impossible. On the other hand, simulations are not as close to reality as experiments due to simplifications in the mathematical models. Nevertheless, for the approach described in this paper they are beneficial, since they allow changing material properties, and changing experimental procedures at nearly no cost. They can thus be used to achieve a more generalized correction of thermal inertia effects.

Based on these considerations, a simulation approach is chosen in which a large number of simulations are carried out once and the results are subsequently used in a correction function fitted to the outcomes of the simulations.

2.4.1. Virtual solar field simulation tool

The Virtual Solar Field software (VSF) is used as a simulation tool to calculate the time delay between two temperature signals at two consecutive temperature sensors. The VSF is a transient simulation tool for line focus solar thermal energy systems with single-phase heat transfer fluid. The tool can model an entire solar field and couples hydraulic and thermal solvers. It is based on transient heat and mass balances for the fluid and wall elements of pipe sections discretized along the collector loop. Typical cell sizes for this application are in the range of 10 m. The VSF is also equipped with a solar field control, which allows the loop output temperature to be maintained at a predefined set point. Detailed information about the tool and the governing equations can be found in [13–16].

Model simplifications with impact on the temperature runtime are discussed in the following. The model is one-dimensional in flow direction, which means there is no radial temperature distribution. Since the flow in the solar field is typically turbulent, a flat radial temperature profile can be assumed and the simplification reflects reality well. The fluid is modeled as incompressible, therefore the density and heat capacity are functions of the temperature only. The axial heat conduction in the fluid is neglected, since very high Nusselt numbers indicate that convection in the pipe flow dominates the heat transfer. The pipe material is modeled with constant density ρ_{Pipe}, heat capacity $c_{\mathrm{p,Pipe}}$, and thermal conductivity λ_{Pipe} over the relevant temperature range. The absorber tubes are modeled without radial temperature distribution. According to Noureldin [16] the typical flow conditions in an absorber tube result in low Biot numbers between 0.02 and 0.17. This means that the heat transfer between the pipe wall and the fluid dominates and the

temperature difference within the pipe wall is negligible. The axial heat conduction in the pipe wall is neglected, since Noureldin [16] showed that this heat transfer process is less than 0.0001 % of the convective heat transfer to the fluid. The thermal loss of the absorber tube to the surroundings is calculated with an empirical relation as a function of the average absorber temperature as introduced by [17].

2.4.2. Simulation setup

Multiple VSF simulations with changing parameters for a single loop are performed. Parameter variations include two heat transfer fluids, irradiance, loop lengths, varying defocusing, and material parameters like density and heat capacity of pipe wall and fluid. The parameters are kept constant during the simulation unless otherwise specified. One loop is discretized with 52 cells since sufficiently good agreement with an analytical comparison model is obtained in the work of [16]. Depending on the simulated loop length the discretization corresponds to a cell size of 10 m to 16 m. The loop consists of four collectors connected in a row and the artificial temperature disturbance is induced by defocusing the first collector. The defocusing follows a step signal, i.e., the focus is changed instantaneously within a time step. The temperature at the center of collectors 2 and 3 are used for the detection of the time shift of the signal. These locations are chosen, because sensor signals are usually available for this location in a commercial parabolic trough field [1], and they are closest to the temperature disturbance caused by the first collector.

The fluid runtime between the two temperature sensors represents the target variable to be calculated by considering the temperature runtime and other parameters. From the VSF simulation the mass flow at the loop inlet is available. The respective fluid runtime $t_{\mathrm{Fluid2,3}}$ is given by

$$t_{\mathrm{Fluid2,3}} = \frac{\rho_{\mathrm{Fluid2,3}} \cdot l_{2,3} \cdot A_{\mathrm{Pipe}}}{\dot{m}} \tag{4}$$

where $\rho_{\mathrm{Fluid2,3}}$ and $\dot{m}$ are the mean fluid density and mass flow between the sensors 2 and 3 during the time the temperature signal is traveling from sensor 2 to 3. The variable $l_{2,3}$ is the distance between sensor 2 and 3 and A_{Pipe} represents the flow cross section. The consideration of varying density and mass flow is important because the defocusing procedure changes the temperature and thus the density. As the fluid volume contracts, the local mass flow between sensor 2 and 3 is also reduced.

3. Results and discussion

Within this paragraph the previously presented method of flow determination using a temperature disturbance signal and two consecutive temperature sensors is used in order to directly determine the absolute values of the fluid runtime. The challenge here is to determine the fluid runtime of a single loop from the runtime of the temperature signal. In order to do so, the thermal inertia of the pipe wall is taken into account.

3.1. Parameter space investigated

The input parameters of the simulation were varied over a wide range in order to achieve a broad applicability of the results. Table 1 provides an overview of the input parameters for two different fluids used in the simulation, Therminol-VP1 and Solar Salt. The direct normal irradiance (DNI) is varied between 600 W m^{-2} and 1000 W m^{-2}, which is typical for the normal operation mode of a parabolic trough plant. The density and heat capacity of the pipe material are varied between 7000 kg m^{-3} and 8600 kg m^{-3} and 460 J kg^{-1} K^{-1} and 570 J kg^{-1} K^{-1}, which cover typical values of the high-temperature steels used. To investigate the influence of different temperature gradients ΔT, the amplitude of the defocusing is varied resulting in a remaining focus of 0.01 (nearly defocused) to 0.8 (only 20% reduced heat input). The focus values of 0.01, 0.2, 0.4, 0.6, and 0.8 result in mean ΔT values of 26.7 K,21.6 K,16.2 K,10.8 K,5.4 K for Therminol-VP1 and 57.2 K,45.8 K,34.4 K,23.1 K,11.6 K for Solar Salt. Loop lengths are varied within approx. ±10% with a mean length of 600 m for thermal oil systems and 760 m for molten salt systems. The collector used for thermal oil is a EuroTrough type [18] and for the molten salt system a HelioTrough 2.0 collector [19]. They differ significantly in length, aperture width, and efficiency but are typically used in combination with thermal oil, and molten salt. Both systems use Schott PTR 70 receivers.

Table 1
Parameters of VSF simulations with Therminol VP-1 and Solar Salt. Pipe material properties assume X6CrNiTi18-10 steel for oil systems and X8CrNiTi18-10 steel for molten salt systems and are taken from [20]. The properties of the different steel types are similar in the temperature range under consideration.

Fluid		Therminol VP-1 [21]	Solar Salt [22,23]
DNI	[W/m²]	600, 700, 800, 900, 1000	
ρ_{Fluid}	[kg/m³]	759.7 @350 °C	1821.3 @420 °C
ρ_{Pipe}	[kg/m³]	7000, 7400, 7800, 8200, 8600	
$c_{\mathrm{p,Fluid}}$	[J/(kg K)]	2454.7 @350 °C	1519.7 @420 °C
$c_{\mathrm{p,Pipe}}$	[J/(kg K)]	460, 487.5, 515, 542.5, 570	
λ_{Fluid}	[W/m]	8.65×10^{-2} @350 °C	5.16×10^{-1} @420 °C
η_{Fluid}	[Pa s]	1.83×10^{-4} @350 °C	1.63×10^{-3} @420 °C
T_{in}	[°C]	293	
T_{out}	[°C]	393	550
Focus	[-]	0.01, 0.2, 0.4, 0.6, 0.8	
Loop length	[m]	540, 570, 600, 630, 660	680, 720, 760, 800, 840
Collector	[-]	EuroTrough [18]	HelioTrough 2.0 [19]
Receiver	[-]	Schott PTR 70 [17]	

3.2. Model fit

The results of multiple simulations with varying parameters are combined to create a generalized correction function which solves the inverse problem of determining the fluid runtime from the measured runtime of the temperature signal. In order to keep the correction function simple and at the same time include all influencing parameters a multiple linear regression approach is chosen to map the measured temperature runtime to the fluid runtime. The results obtained by Kraft et al. [11] show that a linear approach is well suited for this type of correction. The influencing parameters describe the parameter space of the transient simulations with the model simplifications described above. With this the correction function has the form:

$$t_{\mathrm{Fluid}}(t_{\mathrm{Temp}}, l, \Delta T, C_{\mathrm{vol}}, \varepsilon) = c_0 + c_1 \cdot t_{\mathrm{Temp}} + c_2 \cdot l + c_3 \cdot \Delta T + c_4 \cdot C_{\mathrm{vol}} + \varepsilon \tag{5}$$

The parameters c_0, c_1, c_2, c_3, c_4 are fitted with a least squares approach using the simulation results, minimizing the error term ε. If these parameters are known the actual fluid runtime t_{Fluid} can be calculated from the measured temperature runtime t_{Temp}, for different distances between the temperature sensors l, different HTF temperature changes ΔT, and different volumetric heat capacities of the pipe material C_{vol}. This makes the approach applicable to loops with different designs, levels of defocusing, and pipe materials.

For Therminol-VP1 and Solar Salt, a separate correction function was fitted to each of the simulation data. This is necessary because the boundary conditions with these two fluids differ significantly. Table 1 shows that the loop outlet set point temperature is 393 °C for thermal oil and 550 °C for molten salt systems. An alternative fitting approach with the fluid as additional parameter results in significantly larger confidence intervals for a combined model compared to single models for each fluid.

The coefficients of the correction function from Eq. (5) are given in Tables 2 and 3 together with their confidence bounds for a 68.3% confidence interval. The R^2 value

$$R^2 = 1 - \frac{\sum_i (y_i - \hat{y}_i)^2}{\sum_i (y_i - \bar{y})^2} \tag{6}$$

Table 2
Coefficients for runtime correction for thermal oil setup. Confidence bounds are calculated with a 68.3% interval. High t-values and rel. parameter influence indicate that t_{Temp} is the most important parameter for the model. R^2 values close to 1 and low mean absolute percentage errors (MAPE) indicate a very good fit.

	Therminol VP-1			
	coefficients		t-value	rel. parameter influence
c_0 [s]	1.030e+01	±6.034e-02	170.84	–
c_1 [−]	8.585e-01	±3.071e-04	2798.08	88.3 %
c_2 [s m^{-1}]	−5.636e-03	±3.211e-04	−17.57	0.6 %
c_3 [s K^{-1}]	−4.154e-02	±4.514e-04	−92.09	2.9 %
c_4 [s^3 K m kg^{-1}]	−2.139e-06	±8.123e-09	−263.48	8.3 %
R^2			0.9996	
MAPE			0.276 %	

Table 3
Coefficients for runtime correction for molten salt setup. Confidence bounds are calculated with a 68.3% interval. High t-values and rel. parameter influence indicate that t_{Temp} is the most important parameter for the model. R^2 values close to 1 and low mean absolute percentage errors (MAPE) indicate a very good fit.

	Solar Salt			
	coefficients		t-value	rel. parameter influence
c_0 [s]	8.643e+00	±6.686e-01	12.94	–
c_1 [-]	1.004e+00	±1.298e-03	774.17	91.2 %
c_2 [s m^{-1}]	1.729e-02	±2.695e-03	6.42	0.7 %
c_3 [s K^{-1}]	2.071e-02	±2.543e-03	8.15	1.0 %
c_4 [s^3 K m kg^{-1}]	−5.650e-06	±9.077e-08	−62.29	7.1 %
R^2			0.9952	
MAPE			0.985 %	

is used as a metric for the quality of the fit. It is close to 1, which indicates the high accuracy of the fit for both fluids. The mean absolute percentage error

$$MAPE = \frac{1}{n}\sum_{i=1}^{n}\frac{y_i - \hat{y}_i}{max(\epsilon, |y_i|)} \tag{7}$$

is sensitive to relative errors and since it is a percentage value it is not changed by scaling of the quantity. The number of observations is n, y_i is a single observation from the transient simulation, $\hat{y}_i$ is a single model prediction from the linear regression fit, and ϵ is an arbitrarily small but strictly positive number, which is chosen if $y_i = 0$. The $MAPE_{\text{Therminol VP-1}} = 0.276\%$ and $MAPE_{\text{Solar Salt}} = 0.985\%$ values are very low and show, in accordance with the R^2 metric, the good agreement of the linear regression fit with the transient simulations.

3.3. Correction function illustrated in practitioner plots

In order to easily infer the volumetric flow directly from the time difference of the temperature signals, a so-called practitioner plot can be used, see Figs. 4 and 5. The plots represent a special case of the model fits with full defocusing, resulting in a focus factor of $f = 0.01$. The pipe material properties are also kept constant for these plots ($C_{\mathrm{vol}} = const.$). This special case is intended to represent the most common use case in commercial parabolic trough fields.

The marked points of the plots represent single results from the VSF simulations, the dashed lines show the results obtained with the help of the linear regression model from above.

3.3.1. Selection of the amplitude of the temperature disturbance signal

The plot for thermal oil with $f = 0.01$ shows very good agreement between single VSF simulation results and the created linear regression model for all running lengths and temperature runtimes. With a less intensive defocusing of $f > 0.01$ a similar agreement is obtained (plot not shown here). For the application of this procedure it can be advantageous to use a defocusing of $f > 0.01$. On the one hand, very good results can be achieved in the determination of the fluid runtime and, on the other hand, the temperature drop is small, thus minimizing the disturbing influence on the operation of the power plant. Considering this, less than complete defocusing seems to be best suited for the use of the approach to determine the volumetric flow rate from the temperature runtime. For the practical application of the method, an angular deviation from the solar angle can be determined for the defocusing process depending on the acceptance angle of the parabolic trough collectors. For a typical EuroTrough collector the focus rates 0.01, 0.2, 0.4, 0.6, and 0.8 can be achieved by an angular deviation of approx. > 3.0°, 2.6°, 2.0°, 1.5°, and 0.7°.

For molten salt systems the practitioner plot in Fig. 5 shows good accordance between single VSF simulation results and the created linear regression model. The edge values of the linear regression fit at low temperature runtimes t_{Temp} are slightly lower and at high t_{Temp} values

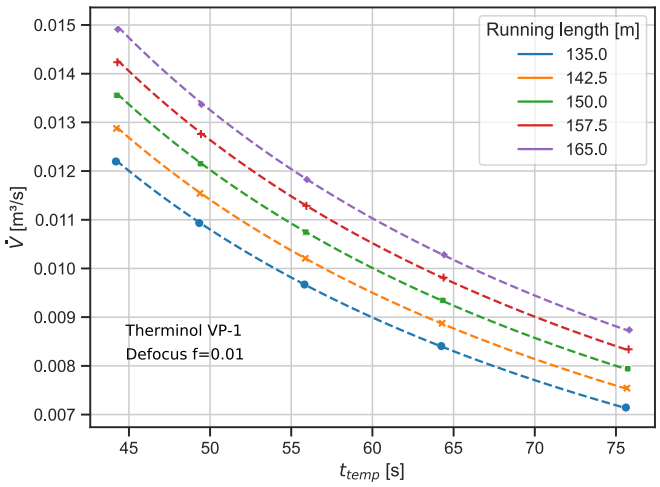

Fig. 4. Volume flow rate over temperature runtime t_{temp} for a variation of running lengths. Plot valid for fluid Therminol VP-1 and excitation by complete defocusing ($f = 0.01$). Marked points show VSF simulation results, dashed lines model fit according to Eq. (5) and Table 2.

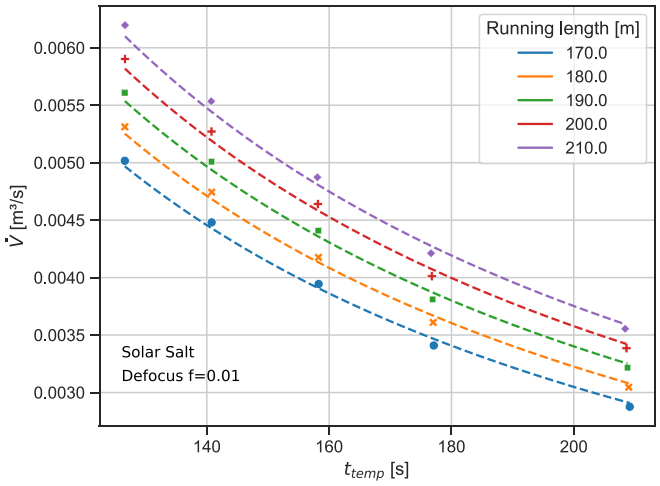

Fig. 5. Volume flow rate over temperature runtime t_{Temp} for a variation of running lengths. Plot valid for fluid Solar Salt and excitation by complete defocusing ($f = 0.01$). Marked points show VSF simulation results, dashed lines model fit according to Eq. (5) and Table 3.

slightly higher compared to the results from the VSF simulations. The results with a higher focus of $f = 0.8$ show contrasting results with a slight overestimation at low temperature runtimes and a slight underestimation at high temperature runtimes (plot not shown here). This indicates that the linear regression model for these parameter combinations is not fully able to reproduce the results from the VSF simulations. The VSF simulations thus capture effects that cannot be covered by the simple linear regression model with the selected parameters. The best accordance between single VSF simulation results and the created linear regression model can be obtained with defocusing rates of $f = 0.4$ or $f = 0.6$. Selecting one of these defocusing rates in the practical application minimizes the error of the correction function and is therefore beneficial for the use of the method.

3.3.2. Notes on using the correction function in the practitioner plots

For the use of the plots, constant irradiation and flow conditions are assumed during the measurement of the temperature runtime. In addition, the distance of the temperature sensors must be known and it must be possible to generate and record temperature steps in the loop. The plots were generated under the assumption that a temperature disturbance is generated at collector 1 in the loop by defocusing and that this is measured at the following collectors 2 and 3. The time difference of the temperature steps can be calculated with the procedure from Section 2.3. Knowing the temperature runtime t_{Temp} now makes it possible to easily read the corresponding volumetric flow from Fig. 4 for thermal oil, or with Fig. 5 for a molten salt system.

These practitioner plots therefore provide a simple possibility to read the corresponding volume flow from a pure temperature measurement in the solar field without additional instrumentation. This allows them to be used directly in the solar field, for example for loop-wise performance monitoring.

3.4. Application of the method with spatially resolved irradiance data

In the following, the applicability of the method for real, spatially resolved and time-varying irradiation data will be tested with transient VSF simulations for thermal oil systems. The aim is to test how the method performs with slightly fluctuating irradiance and with transient irradiance situations in the morning and evening. For this purpose, DNI maps are used, which are recorded with a ground-based cloud camera system. The measurement system and the processing of DNI maps are described by [24]. The spatially resolved irradiance data are used as effective irradiance

$$G_{\mathrm{eff}} = DNI \cdot \cos(\theta_i) \cdot IAM \tag{8}$$

in the VSF simulations. With the DNI values multiplied by the cosine of the incidence angle θ_i and the incidence angle modifier (IAM). The DNI data were recorded at the Plataforma Solar de Almería (PSA) in Tabernas, Spain. They contain measurement values for each solar collector unit with a temporal resolution of one second. The resolution is scaled down linearly from cloud camera images with a resolution of 30 s.

Clear sky conditions without cloud cover are used for this test. This selection represents the frequently occurring operating conditions of a solar thermal power plant in regions of the world with high levels of solar irradiation. To achieve such conditions, disturbing effects caused by short-term changes in cloud cover, which abruptly change the irradiance and thus the heat input to the absorber tubes, are excluded. Such situations would lead to inhomogeneous temperature signals in the collector circuit, which would make it difficult to determine the temperature runtime. The tests are carried out using data from 08/09/2015 and 28/11/2015, measured at the PSA site. The spatial mean G_{eff} values for the two days are shown in Fig. 6. Data from 28/11/2015 show a clear-sky day with low sun angles close to the winter solstice. Data from 08/09/2015 show a high sun position at the end of summer with periods of reduced DNI due to cloud cover, these periods were excluded from this test.

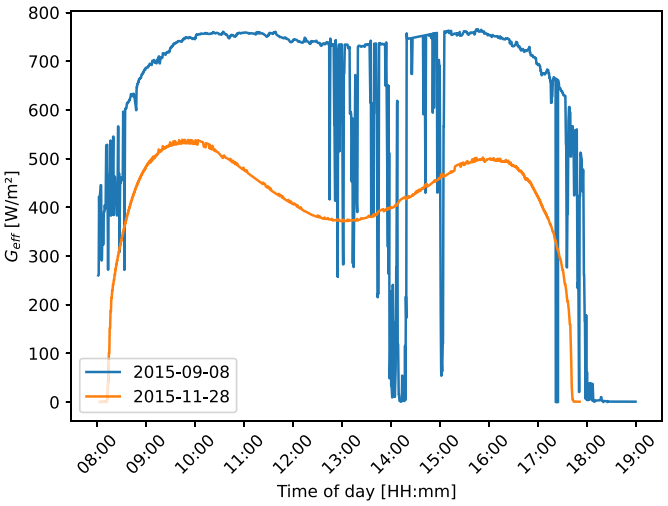

Fig. 6. Mean values of spatially resolved G_{eff} map from cloud camera images for 08/09/2015 and 28/11/2015 for PSA location.

The flow determination was carried out at three irradiance situations per test day: an approximately stationary G_{eff} at solar noon and two non-stationary situations, one with increasing G_{eff} in the morning, and one with decreasing G_{eff} in the evening. The first situation is important to quantify the performance of the method in stationary irradiation situations. The latter aims to quantify the performance of the method in transient irradiation conditions. In situations with changing G_{eff}, the fluid flow in the parabolic trough system also changes, as the controller tries to maintain a stable outlet temperature. If the fluid flow is determined during this period using the temperature transit time method, the flow rate determined is an average value over the measurement time of the method. In the VSF simulations the first collector in the loop is turned out of the focus for 200 s, with starting times 9:00, 12:00, and 16:50 on 08/09/2015 and 8:30, 13:00, and 16:45 on 28/11/2015. This defocusing creates a temperature signal, which is used to calculate the fluid runtime using a correction function, as described in Section 3.2. The VSF simulations are carried out with the same temporal resolution of one second as provided by the irradiance maps.

For all irradiance situations under investigation the reference fluid runtime from the VSF simulations is compared with the fluid runtime calculated from the temperature signal. Table 4 shows the results for the two test days, together with the absolute and percentage differences between the modeled fluid runtime value from the simulations and the calculated value from the temperature signal. The difference between the values is small with a minimum difference of 0.03% for a decreasing irradiance situation on 08/09/2015 and a maximum difference of −2.73% for the decreasing irradiance situation on 28/11/2015. On both days the stable irradiance situations show similar percentage

Table 4
Fluid runtime from VSF simulations with thermal oil and spatially resolved irradiance maps as input. Fluid runtime calculated from temperature curves ($t_{Fluid,cal}$) shows small differences compared to the transient simulations ($t_{Fluid,mod}$). Temperature runtime (t_{Temp}) as reference shows the effect of the correction function.

Date	G_{eff} situation	t_{Temp} [s]	$t_{Fluid,mod}$ [s]	$t_{Fluid,cal}$ [s]	Diff. [s]	Diff. [%]
08/09/2015	increasing	66.39	56.04	56.75	−0.71	−1.26
	stable	61.33	51.53	52.41	−0.88	−1.71
	decreasing	62.56	53.48	53.46	0.02	0.03
28/11/2015	increasing	133.30	114.38	114.30	0.08	0.07
	stable	128.02	108.01	109.77	−1.76	−1.63
	decreasing	103.45	86.26	88.62	−2.36	−2.73

differences of −1.63% to −1.71%. For increasing and decreasing irradiance situations no consistent difference can be observed.

These results show that the small, high-frequency changes in irradiance on a clear sky day have no disturbing influence on the method presented in this paper. The reason for this probably lies in the thermal inertia of the system and in the fact that the method determines a value for a period of time specified by the fluid transit time. This dampens the changes in irradiance, and the disturbances are averaged out. Slow changes in irradiance, such as those that occur in the morning and evening, lead to a simultaneously changing fluid flow in the system control. However, with a comparatively fast measurement time of less than two minutes, the measurement method presented is little affected by these irradiance changes. In addition, the irradiance does not change abruptly. The method presented is therefore also able to determine a reliable mean value of the fluid runtime in these situations. This shows that differences in the fluid transit time between simulation and those calculated from the temperature runtime of considerably less than 3% can be achieved. However, it must also be mentioned that although real measured and spatially resolved irradiance values are used in these investigations, the parabolic trough system is represented with the help of simulation data.

3.5. Application of the method in the andasol-3 parabolic trough plant

To test the method developed here in a real operating environment, defocusing tests from the Andasol-3 power plant, recorded on January 19, 2023, are used. The solar field of the plant consists of four symmetric subfields, each consisting of 38 loops and four collectors in each loop. During the tests, all first collectors of each loop of the entire solar field were defocused simultaneously three times at noon. The first time at 12:25, the second time at 13:20, and the third time at 14:10, for about 90 s each time. The DNI during the tests is approximately constant at 1012, 1016, 1002 W m^{-1} and the HTF flow is also approximately constant during each test period.

The defocusing causes a temporary decrease in solar power and a temperature drop can be measured in the downstream temperature sensors. Fig. 7 shows an example of the temperature signal for one representative loop. The temperature drops due to the defocusing of the first collector (LC11) can also be seen in the following sensors (LD11, LD12, LC12) with a time delay. In contrast to the investigations in the previous sections, the temperature runtime between the sensors at the center of collectors 3 and 4 is used for the evaluation in this section.

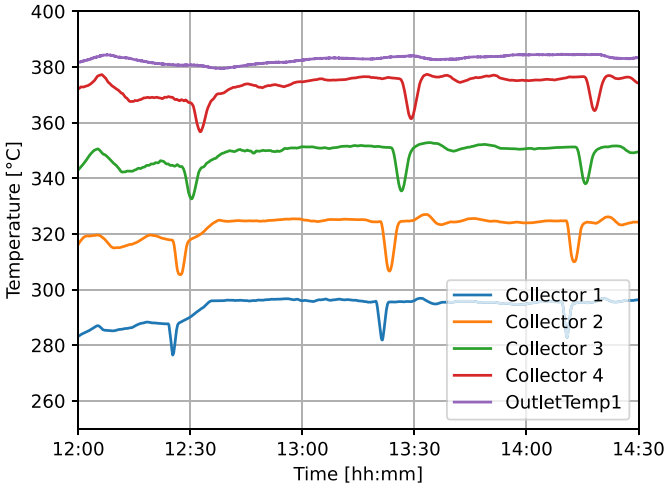

Fig. 7. HTF temperatures measured in the center of the collector and at the outlet of the subfield (OutletTemp1), illustrated with data from loop 28 in the southwestern subfield. The steep temperature drops in the sensor signals, starting at 12:25, 13:20 and 14:10, are the result of a defocusing of collector 1.

The distance between these sensors is 150 m, which is covered by the correction function described in Section 3.2. The use of collectors 3 and 4 is necessary because there is a crossover pipe and an extension loop between collectors 2 and 3 in the collector loops of Andasol-3, which would require new simulations with the VSF model for these specific additional pipe sections.

The signal shift of the temperature drops is determined using the same procedure as shown in Section 2.3. With the correction term from Section 3.2, the fluid transit time t_{Fluid} and with Eqs. (1) and (2) the mass flow of a single loop can be determined.

For the comparison of the method with existing measurements in the Andasol-3 solar field, volume flow measurements from ultrasonic flow meters at the subfield inlets are available, see [10]. The calculated loop flows must therefore be summed up with

$$\dot{m}_{subf} = \dot{V}_{subf,meas} \cdot \rho(T_{subf,in}) = \sum_{loop=1}^{38} \dot{V}_{loop} \cdot \rho(T_{loop}). \tag{9}$$

for the entire subfield in order to compare them with the measurement data. In this analysis, the mass flow is used because the fluid density is temperature-dependent and therefore differs between the two measuring points subfield inlet and collector 3–4 with increasing fluid temperature. Assuming that the mass flow is conserved within one subfield, the summed up flow values of the loops and the measured value at the subfield inlet can be compared. Fluid densities are calculated using a temperature-dependent density correlation from the HTF data sheet [21] and temperature measurements at the flow measurement location. With the three defocusing procedures in four subfields, a total of twelve experiments can be extracted from the data to compare the developed procedure with the subfield flow measurements.

A manual review of the 12 experiments × 38 collectors = 456 defocusing procedures excluded 26 of them for different reasons: in two cases, collectors were not defocused; in five cases, the temperature signals were erroneous; and in 19 cases, the temperatures were unstable. The transit time measurement method is not applicable in these cases. Table 5 shows an overview of the experiments and the data from the loops that were filtered out for the investigation. In cases where a filter is applied the flow data is replaced by the calculated flow values of the loop on the opposite side of the subfield header. Due to the approximately equal pipe length from the entrance of the subfield, it is assumed that comparable flow conditions prevail in the opposite loops.

Fig. 8 shows the comparison of the mass flow calculated with the time offset method compared to the measured values at the subfield entrance. The time offset method follows the variation of the mass flow in the different experiments very well, but it systematically underestimates the values across all experiments. This results in error metrics root mean squared error $RMSE = 8.22$ kg s^{-1} and $MAPE = 6.15\%$.

Table 5
Overview of defocusing experiments performed at the Andasol-3 plant on January 19, 2023. Calculated flow rates of the filtered loops are replaced by the flow rates of the opposite loops.

Experiment	Subfield	Time	Filter applied to loop number
1	1	12:25	1: not defocused; 11: instable temperature
2	1	13:20	1: not defocused; 24, 36, 30: instable temperature
3	1	14:10	26, 36: instable temperature
4	2	12:25	23,28: instable temperature; 37: erroneous signals
5	2	13:20	5, 23: instable temperature; 37: erroneous signals
6	2	14:10	5: instable temperature; 37: erroneous signals
7	3	12:25	20: erroneous signals
8	3	13:20	29: instable temperature
9	3	14:10	no filter required.
10	4	12:25	22: erroneous signals
11	4	13:20	26, 29, 34, 36: instable temperature
12	4	14:10	17, 21, 29: instable temperature

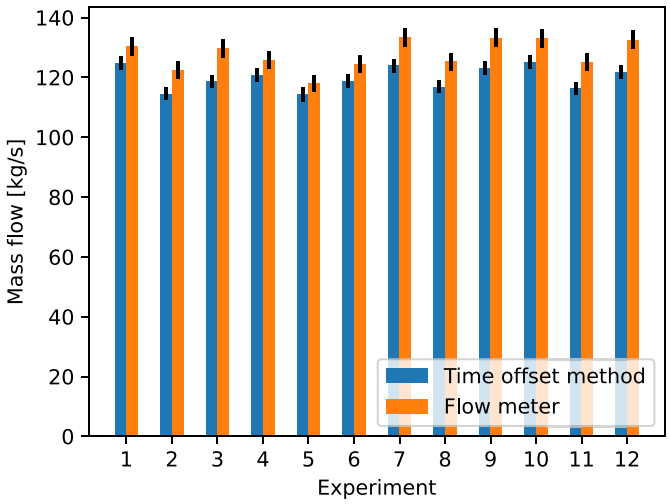

Fig. 8. Mass flow in the subfield calculated using the time offset method compared to flow meter readings. Error bars of flow meter readings according to [10], error bars of the time offset method according to uncertainty estimation in Appendix A.

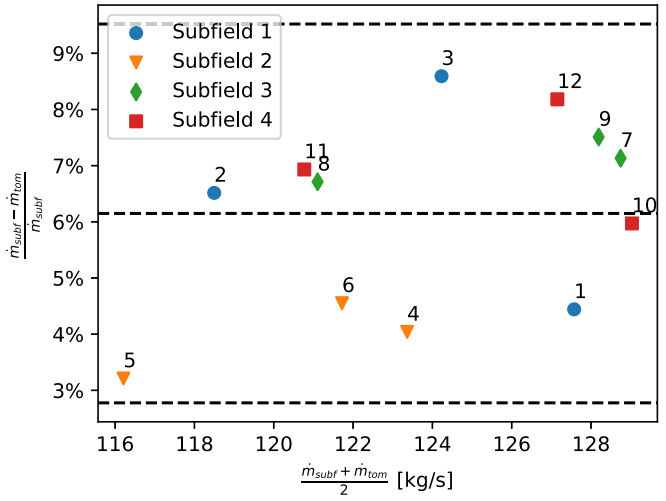

Fig. 9. Deviation of subfield mass flow calculated with the time offset method $\dot{m}_{tom}$ and flow measurement $\dot{m}_{subf}$ over the mean of these values. Dashed lines indicate mean offset and ±1.96 times the standard deviation of the mean. Numbers indicate the experiment number.

The deviation of the mass flow values can be investigated in detail with a scatter plot of the deviations over the mean values, see Fig. 9. The scatter plot shows a systematic offset of approx. 7.9 kg s^{-1} between measured and calculated data. Despite this offset all values are within the 95% confidence interval between the boundaries of ±1.96 times the standard deviation of the mean. This demonstrates the good agreement between the mass flow determined using the time offset method and the measured mass flow.

This first application of the flow determination method to a commercial parabolic trough power plant during operation shows the feasibility of the procedure and a good agreement with the measured subfield mass flows. The procedure shows a systematic deviation in all experiments examined. Two fundamental sources of error come into consideration for these deviations:

- Uncertainty of the fluid density, which is needed to determine the mass flows. Data from the HTF data sheet [21] are used here, as there were no recent laboratory measurements of the density available.
- Uncertainty of the flow meter installed at the subfield inlet of the Andasol-3 plant. No recent calibration is available for this instrument.

The investigation of these influences can be the subject of future studies. Taking into account the subfield flow measurements, an additional linear correction can be applied to the results of the time offset method and the deviation can be reduced to very low values of $RMSE = 2.48$ kg s^{-1} and $MAPE = 1.74$ %.

These tests are the first validation of the developed process in a realistic application scenario at a commercial parabolic trough power plant.

3.6. Impact of the temporary defocusing on plant operation

Within this paragraph the influence of the temporary defocusing on plant operation is investigated on the basis of three effects: The reduction in solar energy yield due to defocusing, the influence on the outlet temperature in the subfield due to the temperature drops, and the change in volume of the HTF due to the temperature change.

During the defocusing procedure the first collector is rotated out of focus and the solar energy is no longer concentrated on the absorber tube of the first collector. For a typical solar field with four collectors in one loop, the energy input is reduced by 25% during the defocusing. For a simple estimate, a constant irradiation over ten hours is assumed. With a defocus procedure of 90 s every 30 min, the energy yield decreases by 1.25% during the day. This value is considered to be negligibly small because the process can be combined with dumping processes, making the losses irrelevant.

The influence of the defocusing procedure on the outlet temperature in the subfield is due to the fact that after the HTF has run through the individual loops, it is collected in the subfield header pipe. Due to the different pipe lengths, seen from the subfield entrance, the temperature drops overlap with a time delay and only a slight temperature drop can be measured at the subfield outlet. The influence of the defocusing method on the outlet temperature in the subfield can be seen in Fig. 7 for subfield 1. The moderate temperature decrease is in the range of 2 K within 5 min, followed by an increase to the initial value. This temperature decrease is within the range of usual fluctuations, as they can also arise from changing cloud situations, and therefore does not indicate any danger for safe solar field operation.

Another effect that must be taken into account in this process is the influence of the short-term temperature change on the fluid volume and the associated influences on the flow velocity. The temporary defocusing partly halts the thermal expansion of the fluid as it flows through the loop. This can reduce the volume flow in the other loops of the subfield and can lead to a short increase in HTF temperature due to the flow reduction. On the basis of the non-defocused loop 1 in experiment 1 and 2 (see Table 5), a temperature increase of approx. 9 K can be observed on the first collector, while the other collectors in the subfield are temporarily defocused. In the worst case, this short-term temperature increase can lead to overheating of the fluid or to a safety defocusing. To prevent this, the defocusing in the solar field should be carried out with a time delay so that there are no superimposed effects of the change in volume of the fluid. It is assumed that this effect is smaller in systems with solar salt due to a lower temperature-dependent density change of the fluid.

4. Conclusions

The absence of flow measurements in typically instrumented parabolic trough loops makes it impossible to easily determine flow for the purpose of calculating the performance of a loop. The proof-of-concept study presented in this paper uses the temperature sensors at the collectors to measure the runtime of a temperature signal and infer the runtime of the fluid. It is therefore not dependent on additional measurement instrumentation and only requires data analysis

using the available measurement equipment. The approach can therefore be applied to existing parabolic trough loops at nearly no additional cost.

The method was validated in a realistic application scenario with data from the parabolic trough power plant Andasol-3 and shows a mean absolute percentage error of 6.15% compared to the measured subfield mass flow. If the goal is only the relative distribution of the mass flow in the individual loops, the error of the method is smaller, since uncertainties are canceled out for identically constructed loops. The use of a correction function that takes into account the influences of the pipe wall substantially improves the results, especially for thermal oil. If the temperature runtime is directly used as surrogate for the fluid runtime the error would be too large to be used for the determination of the fluid runtime. The method was developed based on a large number of transient simulations and validated using subfield flow measurements. The simulation-based approach avoids the need for individual calibration of the correction function, which would otherwise have to be repeated for each new configuration. The simulations include simplifications of the processes in a parabolic trough loop. Although the simplifications are considered to be of minor importance, it is a logical next step to validate the results of this study with flow measurements at each loop in a parabolic trough field under realistic operating conditions.

The results from this paper can be used in both parabolic trough and linear Fresnel systems, but may also be applied to other pipe flows in process engineering applications. The determination of absolute values of the fluid runtime using a correction function or using one of the practitioner plots only requires an accurate measurement of the temperature runtime. This approach has the potential to help plant operators measure flow in the loops without the need to install additional costly measurement equipment.

CRediT authorship contribution statement

Alex Brenner: Writing – original draft, Software, Methodology, Investigation, Conceptualization. **Tobias Hirsch:** Writing – review & editing, Conceptualization, Funding acquisition. **Marc Röger:** Conceptualization, Writing – review & editing. **Jana Stengler:** Writing – review & editing. **Robert Pitz-Paal:** Supervision.

Declaration of competing interest

The authors declare that they have no known competing financial interests or personal relationships that could have appeared to influence the work reported in this paper.

Acknowledgments

Funded by the Federal Ministry for the Environment, Climate Action, Nature Conservation and Nuclear Safety (BMUKN) based on a decision of the German Bundestag. The authors would like to thank Marquesado Solar for providing the data as part of the AuSeSol-AI project.

Appendix A. Uncertainty analysis for volumetric flow calculations

In order to estimate the uncertainties associated with the approach in this work, typical uncertainties of a field measurement are used in the following and a combined standard uncertainty is determined.

The presented approach has two basic sources of uncertainty. On the one hand the uncertainty of the generated linear regression model and on the other hand the uncertainty of the parameters used in the model. The latter depends in the real application on the measurement equipment and components used and is carried out within this first theoretical estimation with typical uncertainty values for the respective measurand.

The uncertainty of the linear regression fit from Eq. (5) with the coefficients for thermal oil in Table 2, and for molten salt in Table 3 is calculated using the GUM approach [25]. In this approach, the uncertainties of all input variables are used in a measurement model to determine their effect on the final quantity being searched for. The calculation of uncertainty is conducted under the assumption of uncorrelated input quantities and under the assumption of a worst-case scenario. This means that from the multiple simulations, the value chosen is the one that has the largest negative influence on the combined uncertainty. The results with an irradiation of 800 W m^{-2} and collector lengths of 150 m for oil systems and 190 m for molten salt systems are used. The combined standard uncertainty of t_{Fluid} has a confidence interval of 68.3% and is calculated by

$$u_{\mathrm{c}}(y) = \sqrt{\sum_{i=1}^{N} \left(\frac{\partial f}{\partial x_i} \right)^2 u^2(x_i)}. \tag{A.1}$$

The partial derivative $\frac{\partial f}{\partial x_i}$, also called sensitivity coefficient, is calculated for each component of Eq. (5). They describe how the output t_{Fluid} varies with changes in the values of the components of Eq. (5). The uncertainty corresponding to each component is $u(x_i)$. The uncertainty estimation is calculated using the Python symbolic mathematics library `SymPy` [26].

With $C_{\mathrm{vol}} = c_{\mathrm{p,Pipe}} \cdot \rho_{\mathrm{Pipe}}$ the combined standard uncertainty $u_c(t_{\mathrm{Fluid}})$ for uncorrelated input quantities is given by

$$u_{\mathrm{c}}(t_{\mathrm{Fluid}}) = \sqrt{\begin{aligned} &c_1^2 u_{t_{\mathrm{Temp}}}^2 + c_2^2 u_l^2 + c_3^2 u_{\Delta T}^2 + c_4^2 c_{\mathrm{p,Pipe}}^2 u_{\rho_{\mathrm{Pipe}}}^2 + c_4^2 \rho_{\mathrm{Pipe}}^2 u_{c_{\mathrm{p,Pipe}}}^2 \\ &+ c_{\mathrm{p,Pipe}}^2 \rho_{\mathrm{Pipe}}^2 u_{\mathrm{c4}}^2 + \Delta T^2 u_{\mathrm{c3}}^2 + l^2 u_{\mathrm{c2}}^2 + t_{\mathrm{Temp}}^2 u_{\mathrm{c1}}^2 + u_{\mathrm{c0}}^2 \end{aligned}}. \tag{A.2}$$

For the calculation of the combined standard uncertainties of t_{Fluid} for Therminol VP-1 and Solar Salt the uncertainties of each influencing parameter together with the sensitivity coefficients are summarized in Table A.6. For $c_{\mathrm{p,Pipe}}$ and ρ_{Pipe} an uncertainty of 1% of the quantity's value is assumed, for l and t_{Temp} an uncertainty of 0.01 m and 1 s is assumed to be achievable. These assumptions take into account that the steel used is standardized and has a fixed material composition, and that length and temperature measurements can be made with great precision even with simple measuring technology. The minimum value for ΔT is chosen as it represents scenarios with the largest uncertainty. The uncertainty of temperature sensors is mainly caused by the absolute

Table A.6
Parameters for uncertainty estimation of $u_{\mathrm{c}}(t_{\mathrm{Fluid}})$ for Therminol VP-1 and Solar Salt. In both cases the measurement of the time difference of the temperature signals t_{Temp} has the largest influence.

Quantity	Value	$u(x_i)$	$\frac{\partial f}{\partial x_i}$	u_{abs}	u_{rel} [%]
Therminol VP-1					
$c_{\mathrm{p,Pipe}}$	570.0	5.7	−1.84e-2	1.05e-1	8.19%
ρ_{Pipe}	8600.0	86.0	−1.22e-3	1.05e-1	8.19%
ΔT	5.37	1.05	−4.15e-2	4.34e-2	3.39%
l	150.00	0.01	−5.64e-3	5.64e-5	0.00%
t_{Temp}	57.6	1.0	8.59e-1	8.59e-1	**67.07%**
c_0	1.03e+1	6.03e-2	1.00	6.03e-2	4.71%
c_1	8.59e-1	3.07e-4	5.76e+1	1.77e-2	1.38%
c_2	−5.64e-3	3.21e-4	1.50e+2	4.82e-2	3.76%
c_3	−4.15e-2	4.51e-4	5.37	2.42e-3	0.19%
c_4	−2.14e-6	8.12e-9	4.90e+6	3.98e-2	3.11%
Solar Salt					
$c_{\mathrm{p,Pipe}}$	570.0	5.7	−4.86e-2	2.77e-1	8.03%
ρ_{Pipe}	8600.0	86.0	−3.22e-3	2.77e-1	8.03%
ΔT	10.53	1.22	2.07e-2	2.52e-2	0.73%
l	190.0	0.01	1.73e-2	1.73e-4	0.01%
t_{Temp}	163.0	1.0	1.00	1.00	**29.12%**
c_0	8.64	6.69e-1	1.00	6.69e-1	19.40%
c_1	1.00	1.30e-3	1.63e+2	2.12e-1	6.14%
c_2	1.73e-2	2.69e-3	1.90e+2	5.12e-1	14.85%
c_3	2.07e-2	2.54e-3	1.05e+1	2.68e-2	0.78%
c_4	−5.65e-6	9.08e-8	4.90e+6	4.45e-1	12.91%

temperature value. With a small ΔT the temperature within the fluid is maximized during defocusing and with that the uncertainty is maximized. $u(\Delta T)$ is calculated according to the scenario for HTF temperature difference using built-in sensors from [27]. The uncertainties for the coefficients of the linear regression fit $c_0, \dots, c_4$ are determined with a 68.3% confidence interval as shown in Tables 2 and 3.

The relative uncertainty contribution u_{rel} from Table A.6 indicates which of the quantities is mainly responsible for the overall combined uncertainty. For both fluids t_{Temp} has the largest influence, while the effect is even more obvious for Therminol VP-1. This result is in agreement with the statistical analysis in Table 2, where t_{Temp} was also identified as the most important parameter for the linear regression model. This shows that improving the determination of the time difference of the temperature signals has the greatest potential to reduce the combined uncertainty $u_{\mathrm{c}}(t_{\mathrm{Fluid}})$ of the calculated fluid runtime.

The volumetric flow can be calculated by the the volume V of the pipe between the two collectors divided by the calculated fluid runtime t_{Fluid}, see Eq. (1). For the calculation of the combined uncertainty $u_{\mathrm{c}}(\dot{V})$ the uncertainty of d_{i} needs to be included in addition to the quantities for the calculation of $u_{\mathrm{c}}(t_{\mathrm{Fluid}})$. The uncertainty of the inner diameter $u(d_{\mathrm{i}})$ is estimated using the specifications for the outer diameter of the receiver tube $d_{\mathrm{o}} = 70\ \mathrm{mm} \pm 0.3\ \mathrm{mm}$ and the wall thickness $s = 2\ \mathrm{mm} \pm 0.2\ \mathrm{mm}$ given for a RIOGLASS PTR® 70-4 G Receiver [28]. The manufacturing tolerances of the receiver tubes are taken into account with a rectangular probability distribution. The combined uncertainty $u_{\mathrm{c}}(\dot{V})$ is then calculated as shown in Eq. (A.3). The uncertainty contributions are given in Table A.7. For Therminol VP-1 the measurement of the time difference of the temperature signals t_{Temp} has the largest influence. For Solar Salt the inner pipe diameter d_{i} has the largest influence on the combined uncertainty.

With the uncertainty contributions and sensitivity coefficients presented above, the combined standard uncertainty according to Eqs. (A.2) and (A.3) can be determined to the values given in Table A.8. The relative values refer to average fluid runtimes $\bar{t}_{\mathrm{Fluid}}(\mathrm{Therminol\ VP\text{-}1}) = 48.1$ s and $\bar{t}_{\mathrm{Fluid}}(\mathrm{Solar\ Salt}) = 148.2$ s, as well as the minimal volumetric flows $\dot{V}(\mathrm{Therminol\ VP\text{-}1}) = 0.0107\ \mathrm{m^3\ s^{-1}}$ and $\dot{V}_{\mathrm{Solar\ Salt}} = 0.0044\ \mathrm{m^3\ s^{-1}}$ used in the worst-case scenario.

Table A.7
Parameters for uncertainty estimation of $u_{\mathrm{c}}(\dot{V})$ for Therminol VP-1 and Solar Salt. For Therminol VP-1 the measurement of the time difference of the temperature signals t_{Temp} has the largest influence. For Solar Salt the inner pipe diameter d_{i} has the largest influence on the combined uncertainty.

Quantity	Value	$u(x_i)$	$\frac{\partial f}{\partial x_i}$	u_{abs}	u_{rel} [%]
Therminol VP-1					
$c_{\mathrm{p,Pipe}}$	570.0	5.7	4.06e-6	2.32e-5	6.15%
ρ_{Pipe}	8600.0	86.0	2.69e-7	2.32e-5	6.15%
ΔT	5.37	1.05	9.18e-6	9.60e-6	2.55%
l	150.00	0.01	7.22e-5	7.22e-7	0.19%
d_{i}	0.066	2.89e-4	3.23e-1	9.31e-5	24.73%
t_{Temp}	57.6	1.0	−1.90e-4	1.90e-4	**50.35%**
c_0	1.03e+1	6.03e-2	−2.21e-4	1.33e-5	3.54%
c_1	8.59e-1	3.07e-4	−1.27e-2	3.91e-6	1.04%
c_2	−5.64e-3	3.21e-4	−3.31e-2	1.06e-5	2.82%
c_3	−4.15e-2	4.51e-4	−1.19e-3	5.35e-7	0.14%
c_4	−2.14e-6	8.12e-9	−1.08e+3	8.80e-6	2.34%
Solar Salt					
$c_{\mathrm{p,Pipe}}$	570.0	5.7	1.44e-6	8.21e-6	5.83%
ρ_{Pipe}	8600.0	86.0	9.55e-8	8.21e-6	5.83%
ΔT	10.53	1.22	−6.14e-7	7.47e-7	0.53%
l	190.0	0.01	2.26e-5	2.26e-7	0.16%
d_{i}	0.066	2.89e-4	1.33e-1	3.84e-5	**27.27%**
t_{Temp}	163.0	1.0	−2.98e-5	2.98e-5	21.13%
c_0	8.64e+0	6.69e-1	−2.96e-5	1.98e-5	14.08%
c_1	1.00e+0	1.30e-3	−4.83e-3	6.27e-6	4.45%
c_2	1.73e-2	2.69e-3	−5.63e-3	1.52e-5	10.78%
c_3	2.07e-2	2.54e-3	−3.12e-4	7.94e-7	0.56%
c_4	−5.65e-6	9.08e-8	−1.45e+2	1.32e-5	9.37%

Table A.8
Combined uncertainty of calculated fluid runtime $u_{\mathrm{c}}(t_{\mathrm{Fluid}})$ and volumetric flow $u_{\mathrm{c}}(\dot{V})$ for Therminol VP-1 and Solar Salt.

	Therminol VP-1		Solar Salt	
	absolute	relative	absolute	relative
$u_{\mathrm{c}}(t_{\mathrm{Fluid}})$	0.88 s	1.82%	1.45 s	0.98%
$u_{\mathrm{c}}(\dot{V})$	$2.15 \times 10^{-4}\ \mathrm{m\ s^{-3}}$	2.02%	$5.77 \times 10^{-5}\ \mathrm{m\ s^{-3}}$	1.32%

The combined uncertainties $u_{\mathrm{c}}(\dot{V})$ of the presented approach are three to four times larger than the uncertainties reported for flow measurements with a vortex flow meter $u_{\mathrm{c}}(\dot{V}_{\mathrm{Vortex}}) \approx 0.4\%$, as described by [27]. Calculating the mass flow with the given approach further increases the combined uncertainty since the determination of the fluid density is also subject to uncertainty. Assuming an uncertainty of 1% for the fluid density leads to the uncertainties shown in Fig. 8, with the fluid density accounting for one-third of the combined uncertainty. However, considering that the approach is not used as a replacement for an existing measurement system, but provides a way to determine the volumetric flow only with the built-in measurement equipment, the uncertainties appear acceptable.

Calculation of the combined uncertainty of the volumetric flow $u_{\mathrm{c}}(\dot{V})$:

$$
\begin{aligned}
u_{\mathrm{c}}(\dot{V}) = 1.571 \Bigg(& \frac{0.25 c_1^2 d_i^4 l^2 u_{t_{\mathrm{Temp}}}^2}{\left(c_0 + c_1 t_{\mathrm{Temp}} + c_2 l + c_3 \Delta T + c_4 c_{\mathrm{p,Pipe}} \rho_{\mathrm{Pipe}}\right)^4} \\
& + \frac{0.25 c_3^2 d_i^4 l^2 u_{\Delta T}^2}{\left(c_0 + c_1 t_{\mathrm{Temp}} + c_2 l + c_3 \Delta T + c_4 c_{\mathrm{p,Pipe}} \rho_{\mathrm{Pipe}}\right)^4} \\
& + \frac{0.25 c_4^2 c_{\mathrm{p,Pipe}}^2 d_i^4 l^2 u_{\rho_{\mathrm{Pipe}}}^2}{\left(c_0 + c_1 t_{\mathrm{Temp}} + c_2 l + c_3 \Delta T + c_4 c_{\mathrm{p,Pipe}} \rho_{\mathrm{Pipe}}\right)^4} \\
& + \frac{0.25 c_4^2 d_i^4 l^2 \rho_{\mathrm{Pipe}}^2 u_{c_{\mathrm{p,Pipe}}}^2}{\left(c_0 + c_1 t_{\mathrm{Temp}} + c_2 l + c_3 \Delta T + c_4 c_{\mathrm{p,Pipe}} \rho_{\mathrm{Pipe}}\right)^4} \\
& + \frac{0.25 c_{\mathrm{p,Pipe}}^2 d_i^4 l^2 \rho_{\mathrm{Pipe}}^2 u_{c4}^2}{\left(c_0 + c_1 t_{\mathrm{Temp}} + c_2 l + c_3 \Delta T + c_4 c_{\mathrm{p,Pipe}} \rho_{\mathrm{Pipe}}\right)^4} \\
& + \frac{0.25 \Delta T^2 d_i^4 l^2 u_{c3}^2}{\left(c_0 + c_1 t_{\mathrm{Temp}} + c_2 l + c_3 \Delta T + c_4 c_{\mathrm{p,Pipe}} \rho_{\mathrm{Pipe}}\right)^4} \\
& + \frac{0.25 d_i^4 l^4 u_{c2}^2}{\left(c_0 + c_1 t_{\mathrm{Temp}} + c_2 l + c_3 \Delta T + c_4 c_{\mathrm{p,Pipe}} \rho_{\mathrm{Pipe}}\right)^4} \\
& + \frac{0.25 d_i^4 l^2 t_{\mathrm{Temp}}^2 u_{c1}^2}{\left(c_0 + c_1 t_{\mathrm{Temp}} + c_2 l + c_3 \Delta T + c_4 c_{\mathrm{p,Pipe}} \rho_{\mathrm{Pipe}}\right)^4} \\
& + \frac{0.25 d_i^4 l^2 u_{c0}^2}{\left(c_0 + c_1 t_{\mathrm{Temp}} + c_2 l + c_3 \Delta T + c_4 c_{\mathrm{p,Pipe}} \rho_{\mathrm{Pipe}}\right)^4} \\
& + \frac{d_i^2 l^2 u_{d_{\mathrm{i}}}^2}{\left(c_0 + c_1 t_{\mathrm{Temp}} + c_2 l + c_3 \Delta T + c_4 c_{\mathrm{p,Pipe}} \rho_{\mathrm{Pipe}}\right)^2} \\
& + 0.25 u_l^2 \left(- \frac{c_2 d_i^2 l}{\left(c_0 + c_1 t_{\mathrm{Temp}} + c_2 l + c_3 \Delta T + c_4 c_{\mathrm{p,Pipe}} \rho_{\mathrm{Pipe}}\right)^2} \right. \\
& \left. + \frac{d_i^2}{c_0 + c_1 t_{\mathrm{Temp}} + c_2 l + c_3 \Delta T + c_4 c_{\mathrm{p,Pipe}} \rho_{\mathrm{Pipe}}} \right)^2 \Bigg)^{\frac{1}{2}}
\end{aligned}
\tag{A.3}
$$

References

[1] A. Brenner, T. Hirsch, M. Röger, R. Pitz-Paal, State-of-the-Art measurement instrumentation and most recent measurement techniques for parabolic trough collector fields, Energies 14 (2021) 7166, https://doi.org/10.3390/en14217166

[2] A.B. Bauer, Direct measurement of velocity by hot-wire anemometry, AIAA J. 3 (1965) 1189–1191, https://doi.org/10.2514/3.3098

[3] I.H. Tombach, Velocity measurement with a new probe in inhomogeneous turbulent jets, Ph.D. thesis, California Institute of Technology, Pasadena, California, 1969 https://doi.org/10.7907/V2CR-0Q19.

[4] L.J.S. Bradbury, I.P. Castro, A pulsed-wire technique for velocity measurements in highly turbulent flows, J. Fluid Mech. 49 (1971) 657–691, https://doi.org/10.1017/S0022112071002313

[5] G.-A. Tselentis, An investigation of the principles of operation of the heat-pulse flowmeter, J. Hydrol. 69 (1984) 335–349, https://doi.org/10.1016/0022-1694(84)90172-0

[6] K.P. Termaat, Fluid flow measurements inside the reactor vessel of the 50 MWe Dodewaard nuclear power plant by cross-correlation of thermocouple signals, J. Phys. E Sci. Instrum. 3 (1970) 589–593, https://doi.org/10.1088/0022-3735/3/8/302

[7] V. Casal, G. Arnold, W. Harne, R. Kirchner, H. Kußmaul, H. Miller, Verfahren zur messung örtlicher geschwindigkeiten nach dem prinzip der temperatur-puls-propagations-methode, 1988, https://doi.org/10.5445/IR/270025694

[8] A. Nedumparambil, M. Seiz, D. Bestenlehner, H. Drueck, Temperature based determination of volume flow rates in pipes as a low-cost option for energy measurements of Solar thermal systems, in: D. Renné, E. Weber, C. Hachem-Vermette, E. Frank (Eds.), Proceedings of the ISES Solar World Congress 2021, Freiburg, Germany, International Solar Energy Society, 2021, pp. 1–12, https://doi.org/10.18086/swc.2021.26.05

[9] M. Mehos, H. Price, R. Cable, D. Kearney, B. Kelly, G. Kolb, F. Morse, Concentrating Solar power best practices study (2020) https://doi.org/10.2172/1665767

[10] T. Kraft, G. Bern, M. Schmitz, W. Platzer, Mass flow distribution measurement in concentrated solar power plants via thermal time-of-flight method, Sol. Energy 273 (2024) 112486, https://doi.org/10.1016/j.solener.2024.112486

[11] T. Kraft, G. Bern, S. Gomez, W. Platzer, Experimental Demonstration of a mass flow determination in Concentrated solar systems via collector defocusing using Time-of-Flight method, Sol. Energy 287 (2025) 113194, https://doi.org/10.1016/j.solener.2024.113194, https://www.sciencedirect.com/science/article/pii/S0038092X24008892.

[12] A. Brenner, Condition monitoring for parabolic trough fields, Dissertation, RWTH Aachen, Aachen, 2024 (19 November). https://doi.org/10.18154/RWTH-2024-11194.

[13] K. Noureldin, L.M. González-Escalada, T. Hirsch, B. Nouri, R. Pitz-Paal, Modelling and optimization of transient processes in line focusing power plants with single-phase heat transfer medium, in: AIP Conference Proceedings (Ed.), SOLARPACES 2015, AIP Conference Proceedings, 2016, pp. 070022, https://doi.org/10.1063/1.4949169

[14] K. Noureldin, T. Hirsch, R. Pitz-Paal, Virtual Solar field – an opportunity to optimize transient processes in line-focus csp power plants, in: SolarPACES 2016, vol. 1850, Abu Dhabi, UAE, 2016, https://doi.org/10.1063/1.4984553

[15] K. Noureldin, T. Hirsch, R. Pitz-Paal, K. Noureldin, T. Hirsch, R. Pitz-Paal, Virtual Solar Field—Validation of a detailed transient simulation tool for line focus STE fields with single phase heat transfer fluid//Virtual Solar field - Validation of a detailed transient simulation tool for line focus STE fields with single phase heat transfer fluid, Sol. Energy. 146 (2017) 131–140, https://doi.org/10.1016/j.solener.2017.02.028

[16] K. Noureldin, Modelling and control of transients in parabolic trough power plants with single-phase heat transfer fluids, Dissertation, University, RWTH Aachen 2019 https://doi.org/10.18154/RWTH-2019-10244.

[17] F. Burkholder, C. Kutscher, Heat loss testing of schott's 2008 ptr70 parabolic trough receiver, 2009 https://doi.org/10.2172/1369635

[18] E. Lüpfert, E. Zarza, M. Geyer, P. Nava, J. Langenkamp, W. Schiel, A. Esteban, R. Osuna, E. Mandelberg, Euro trough collector qualification complete - performance test results from psa, in: ISES Solar World Congress 2001 & 2003 Proceedings, 2003, https://elib.dlr.de/99768/.

[19] N. Janotte, G. Feckler, J. Kötter, S. Decker, U. Herrmann, M. Schmitz, E. Lüpfert, Dynamic oerformance evaluation of the HelioTrough® Collector demonstration loop–towards a new benchmark in parabolic trough qualification, Energy Procedia 49 (2014) 109–117, https://doi.org/10.1016/j.egypro.2014.03.012

[20] Matplus GmbH, StahlDat SX professional: steel properties database 2023 https://www.stahldaten.de/de/.

[21] Eastman, THERMINOL® VP-1: Ultrahigh-temperature, vapor/liquid phase fluid 2022 https://www.eastman.com/Literature_Center/T/TF9141.pdf.

[22] A.B. ZAVOICO, Solar power tower design basis document, Revision 0 2001 https://doi.org/10.2172/786629

[23] A. Bonk, S. Sau, N. Uranga, M. Hernaiz, T. Bauer, Advanced heat transfer fluids for direct molten salt line-focusing CSP plants, Prog. Energy Combust. Sci. 67 (2018) 69–87, https://doi.org/10.1016/j.pecs.2018.02.002

[24] B. Nouri, P.M. Kuhn, S. Wilbert, C. Prahl, R. Pitz-Paal, P. Blanc, T. Schmidt, Z. Yasser, L. Ramirez, D. Heinemann, P. Kuhn, L.R. Santigosa, D. Heineman, Nowcasting of DNI maps for the solar field based on voxel carving and individual 3D cloud objects from all sky Images//Nowcasting of DNI maps for the solar field based on voxel carving and individual 3D cloud objects from all sky images, in: SOLARPACES (Ed.), SOLARPACES 2017, vol. 2033, 2017, https://doi.org/10.1063/1.5067196, p. 190011.

[25] Joint Committee for Guides in Metrology, Evaluation of measurement data: Guide to the expression of uncertainty in measurement (2008) https://www.bipm.org/documents/20126/2071204/JCGM_100_2008_E.pdf/cb0ef43f-baa5-11cf-3f85-4dcd86f77bd6.

[26] A. Meurer, C.P. Smith, M. Paprocki, O. Čertík, S.B. Kirpichev, M. Rocklin, A. Kumar, S. Ivanov, J.K. Moore, S. Singh, T. Rathnayake, S. Vig, B.E. Granger, R.P. Muller, F. Bonazzi, H. Gupta, S. Vats, F. Johansson, F. Pedregosa, M.J. Curry, A.R. Terrel, Š. Roučka, A. Saboo, I. Fernando, S. Kulal, R. Cimrman, A. Scopatz, SymPy: Symbolic computing in Python, PeerJ Comput. Sci. 3 (2017) e103, https://doi.org/10.7717/peerj-cs.103

[27] N. Janotte, Requirements for representative acceptance tests for the prediction of the annual yield of parabolic trough solar fields, Dissertation, RWTH Aachen, Aachen, 2012. http://publications.rwth-aachen.de/record/210366 (28 June 2012).

[28] Rioglass Solar Holding, S. A, Rioglass PTR® 70-4G: Specifications stainless steel tube 2023 https://old.rioglass.com/rioglass-ptr704g/.